# Assessing Oscillatory Stability with Dominant Grid-Forming Power Systems for Active Power Imbalances

Skogen, Sander; Torres, José Luis Rueda

**DOI**
10.1109/OAJPE.2025.3571108

**Publication date**
2025

**Document Version**
Final published version

**Published in**
IEEE Open Access Journal of Power and Energy

**Citation (APA)**
Skogen, S., & Torres, J. L. R. (2025). Assessing Oscillatory Stability with Dominant Grid-Forming Power Systems for Active Power Imbalances. *IEEE Open Access Journal of Power and Energy*, *12*, 318-329. https://doi.org/10.1109/OAJPE.2025.3571108

IEEE Open Access Journal of Power and Energy

Received 5 December 2024; revised 20 February 2025 and 8 April 2025; accepted 13 May 2025.
Date of publication 21 May 2025; date of current version 27 May 2025.

*Digital Object Identifier 10.1109/OAJPE.2025.3571108*

# Assessing Oscillatory Stability With Dominant Grid-Forming Power Systems for Active Power Imbalances

**SANDER LID SKOGEN AND JOSÉ LUIS RUEDA TORRES (Senior Member, IEEE)**

Intelligent Electrical Power Grids, Delft University of Technology, 2628 CD Delft, The Netherlands
CORRESPONDING AUTHOR: J. L. RUEDA TORRES (j.l.ruedatorres@tudelft.nl)

**ABSTRACT** As the integration of renewable energy accelerates, ensuring power system stability becomes increasingly critical. This research utilized a Root Mean Square (RMS) synthetic model of the future 380 kV Dutch power system towards 2050 to analyze its oscillatory stability under high renewable penetration and the impact of grid-forming converters under various parametrizations. The presented case study shows that grid-forming (GFM) converters significantly improve frequency stability and damping performance across different perturbations, particularly at higher GFM penetration levels, improving frequency and damping parameters. However, various oscillatory modes present potential stability risks at high penetration levels. The case study also shows minimal differences in controller selection in large-scale models, except under certain conditions. Additionally, the analysis of controller parameters highlighted the critical importance of tuning active power parameters to ensure system stability. The investigation provides essential insights for future power systems, where large-scale integration of renewable energy will necessitate the implementation of converters able to provide ancillary services. The findings emphasize the importance of optimizing GFM converter settings and penetration levels to maintain system resilience, offering valuable guidance for future system planning and regulatory frameworks.

**INDEX TERMS** Dynamic active power management, grid-forming control, frequency stability, oscillatory stability, energy transition, digital model of power systems.

## I. INTRODUCTION

ELECTRIC power systems are the backbone of modern society, supporting essential services and enabling technological advancements. As the global energy transition accelerates, a significant influx of renewable power electronic interfaced generation (PEI) units, particularly solar and wind will be connected to the power system. This shift necessitates advancements in understanding the impact of power electronics on the setup and control of future power systems, ensuring stability and reliability.

Renewable energy sources can be categorized into non-PEI and PEI sources. Non-PEI sources, such as hydropower and biomass, connect directly to the power system, behaving similarly to conventional generators but with challenges such as dependency on natural conditions. In contrast, PEI sources, including wind and solar are connected via power electronics, lacking the inherent inertia of synchronous systems and exhibiting significant variability. These typically require advanced control strategies for integration [1].

The increasing prevalence of PEI sources has led to a decline in system inertia, a critical factor in traditional stability ensurance. This has prompted updates to stability classification frameworks by organizations such as IEEE and CIGRE to address the complexities of PEI-dominant systems [2], [3]. Addressing these challenges requires extensive research and collaboration, particularly in areas such as large-scale energy storage, wide-area control systems, and intelligent system management, all of which are crucial for future power system stability [4], [5], [6].

Another significant challenge with PEI generation is the limited controllability and ancillary services. Traditionally, grid-following (GFL) converters have been used. These converters operate dependent on external power system conditions, relying on external signals for operation usually utilizing phase-locked loops (PLL). GFL converters have

a tendency of worsening stability margins of the system, as they can fail to dampen or amplify sudden disturbances. As PEI sources become more prevalent they become critical for maintaining stability, creating a necessity for operation and control independent of the connected power system. Grid-forming (GFM) converters offer a promising solution, providing voltage and power control independently of the external power system, potentially compensating for the reduced presence of traditional power generation units. These converters have been identified as crucial in integrating large-scale PEI generation. However, further research is necessary to fully understand these technologies, including developing test systems and validation procedures and studying real-world impacts on system stability [7], [8], [9].

This work focuses on the large-scale integration of GFM converters with solar PV and wind resources in the future Dutch power system towards 2050, exploring how different GFM controllers, controller parameters, and controller integration levels impact dynamic stability, particularly during critical events such as load increases, short-circuits, and generator outages. The study is centered on frequency and angular stability while focusing on the damping performance of the system. This study aims to bridge the gap between renewable energy goals and the practical realities of power system operations. The findings provide crucial insights into the viability of future PEI integration and highlight the critical aspects of GFM converter implementation. These contributions will advance the power system stability and control field, supporting modern power systems' continued evolution.

### A. REFLECTIONS FROM the STATE-OF-THE-ART

This section reviews the evolving power system landscape, focusing on current GFM converter system performance advancements. The increasing integration of renewable energy and PEI generation necessitates innovative solutions and large-scale system representations to ensure stability and reliability.

#### 1) GRID-FORMING CONVERTERS

Here three different types of GFM converters and their current state-of-the-art technological provess is highlighted.

One critical difference between GFM and GFL technologies lies in controllability. GFL converters depend on external grid-connected AC signals, making them vulnerable during transient events due to fast-acting system changes. In contrast, GFM converters provide the essential voltage and frequency control needed in PEI-dominant systems independently. Various controllers have been proposed, and the focus will be on three prominent candidates: the Virtual Synchronous Machine (VSM), Synchroverter, and Droop controller. Although the Synchroverter is frequently categorized under VSMs, this analysis treats them as distinct entities, reflecting their separate implementation as controller templates in Power Factory.

##### a: VIRTUAL SYNCHRONOUS MACHINE (VSM)

VSMs mimic traditional synchronous generators, with models ranging from simple droop control to complex synchronous machine models. VSMs bridge the inertia gap in PEI systems, providing synthetic inertia and damping through control techniques combined with power electronics [10], [11]. Although promising, further research is needed on integrating energy storage and refining higher-order models [12], [13], [14], [15], [16].

##### b: SYNCHROVERTER

Synchroverters operate similarly to the VSM; they utilize torque control instead of power, enhancing stability by simulating electromagnetic torque. However, their complexity and poor damping pose challenges, necessitating research into optimizing control systems and integrating energy storage [17], [18], [19], [20], [21], [22], [23].

##### c: DROOP CONTROL

Widely used in microgrids, droop control regulates power through frequency and voltage droop without requiring communication. Its simplicity enables easy implementation but can lead to slower transient responses and potential stability issues during transients [24], [25], [26]. Future research should address these challenges and explore large-scale system studies [27], [28], [29].

Overall, GFM converters are essential for integrating large-scale PEI units, offering potential in ancillary services by mimicking traditional synchronous generators. However, extensive research, pilot projects, and policy development are required to realize their complete potential [30], [31].

## II. METHODOLOGICAL APPROACH

The project's methodological approach was conducted in two steps: modeling and simulation setup. Both steps were done using simulation tools and were based on a synthetic representation of the Dutch power system towards 2050 based on available public information and projections.

### A. SYNTHETIC MODELING

The national scenario (NAT) from the II3050-2 project, an outlook of the Dutch power system towards 2050 was selected as a reference point due to the high levels of projected electrification and relevance in ongoing infrastructure developments [32], [33]. The resulting installed capacities of solar PV (PV), onshore (WOL) and offshore wind (WOZ), flexibility resources, and peak demand levels utilized are highlighted in Fig. 1. Utilizing dispatches of 90% WOZ, 10% WOL, 5% PV, 12% flexibility, and 100% demand for the case study.

The power system model was created in two steps, first utilizing detailed plans from the 10-year public investment plans [34], [35], and secondly, utilizing the projections from the II3050-2 projections towards 2050. This approach allowed for a comprehensive representation of

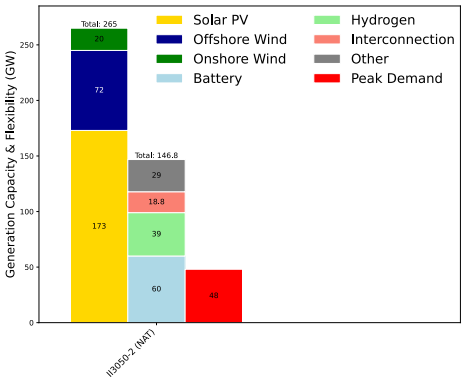


**FIGURE 1. Installed generation, flexibility and demand for the synthetic model.**

future predictions in a large-scale system study, enabling different controller selections and providing a reference for future system parameters.

After implementing the various projects and installed capacities, dynamic controllers were added to the synthetic model. Here, the primary focus was on the PEI generation sources such as solar PV, onshore and offshore wind utilizing GFM and GFL controllers to allow for easy comparison. Various other controllers, such as electrolysers, power-to-heat modules, and load responses, were implemented and set in operation to depict the future power system accurately but were not under further investigation in this project.

The AC interconnections were modeled to reflect the maximum projected inertia constants and kinetic energy levels for Continental Europe toward 2040, as reported by ENTSO-E [36], [37]. These interconnections were represented using synchronous generator models, where active power limits were defined within the dynamic controller. The inertia levels were calculated through a simple conversion based on the following formula:

$$S\ [\text{MVA}] = \frac{E_{\text{kin}}[\text{GVAs}]}{H[\text{s}]} \tag{1}$$

Three GFM controllers were selected and implemented: VSM, Synchroverter, and Droop, due to their availability in PowerFactory's predefined model templates. These were implement in the installed PV, WOL and WOZ soures. An in depth analysis of the three controllers can be found in section III.

Given the uncertainties and lack of specific data in projected infrastructural developments towards 2050, the synthetic model underwent load flow and contingency analyses to ensure realistic system representation. Load flow analysis ensured upgrades on components loaded above 80%, while a 90% threshold was set for N-2 contingency analysis.

Due to these uncertainties, simplifications regarding locations, project sizes, and overall structure were necessary. As future projects become more detailed, it is recommended that the synthetic model be updated to represent the future Dutch power system more accurately. However, it currently

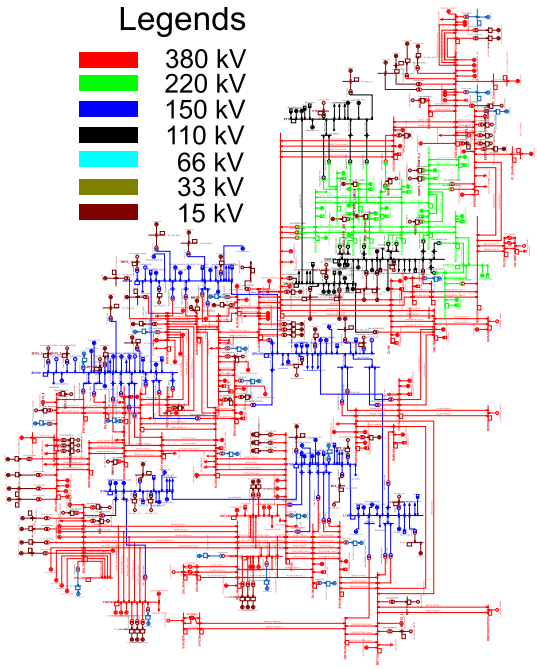


**FIGURE 2. Overview of the Synthetic model highlighting different voltage levels.**

serves as a robust large-scale system representation with various possibilities.

The final system representation in PowerFactory are given in Fig. 2.

### B. SIMULATION SETUP

This section outlines the methodology used to analyze the dynamic stability of the Dutch power system under varying penetration levels, different controller types, and sensitivity to controller parameters for GFM controllers. DigSILENT PowerFactory v2024 SP2, Python 3.12 and Excel 2208 was utilized for the simulations.

The study focuses on high renewable integration scenarios, including offshore and onshore wind and solar PV, managed by different control strategies. The synthetic model was implemented in DIgSILENT PowerFactory, with automated processes via Python and Excel, allowing flexible parameter adjustments and facilitating replication for future research.

The synthetic model setup and simulation process are illustrated in Fig. 3.

Three GFM penetration levels were considered: 25%, 50%, and 85%. One of three GFM converters—VSM, Droop, or Synchroverter—was selected, with base settings or controller parameters adjusted via Python and Excel. Post-simulation, adjustments to penetration levels, controller selection, or parameter modifications were possible enabling a comprehensive assessment of various operational characteristics.

The first analysis compared the three controllers across three disturbances: a short-circuit, load increase, and outage event, with results analyzed using frequency and eigenvalue

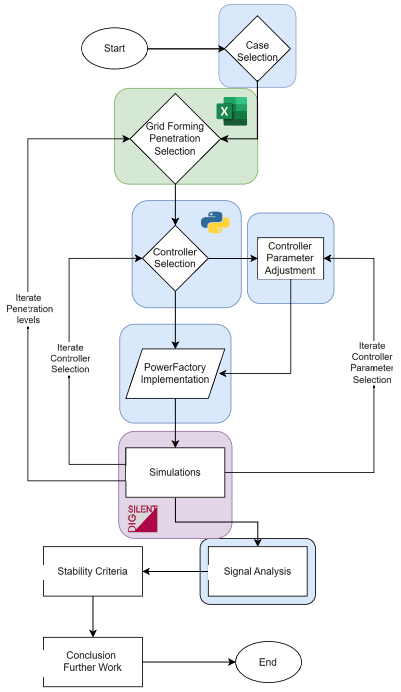


**FIGURE 3. Flowchart illustrating the simulation and analytical process.**

analysis. The eigenvalue analysis was exclusively done on the load event. This study extends previous work, such as [39], by applying these comparisons to a large-scale system representation. Python scripts streamlined the implementation, allowing easier customization. This comparison was conducted for all three GFM penetration levels: 25%, 50%, and 85%.

The second analysis examined the effects of varying GFM penetration levels across all three controllers. This analysis differed from the first by focusing on the impact of different penetration levels rather than comparing the controllers. The differentiation of GFM percentages and controllers was automated through Python, ensuring efficient analysis and reproducibility.

The third analysis conducted a sensitivity study on key controller parameters for the GFM converters identified in section III. Parameters were varied for all GFM converters, assessing their impact on system stability. These parameters and values can be seen in the different controller blocks. A 50% GFM penetration level was used throughout this sensitivity analysis for consistency.

System stability was evaluated through frequency response and eigenvalue analyses to assess the frequency and angular stability of the system. Metrics such as maximum frequency deviation, Rate of Change of Frequency (ROCOF), and settling time were utilized for the frequency assessment. An eigenvalue analysis focusing on damping ratios ($\zeta$) and oscillatory behavior of critical modes assessed the angular stability of the system through the load events. The formulas are given below.

$$\text{ROCOF} = \frac{\Delta f}{\Delta t} \tag{2}$$

$$\text{Max Deviation} = \Delta f_{max} \tag{3}$$

$$\zeta = -\frac{\sigma}{\sqrt{\sigma^2 + \omega^2}} \tag{4}$$

The study simulated three distinct disturbance events—a 2 GW nuclear power plant outage, a short-circuit at one of the tie-lines between the 380 and 150 kV power systems, and a 5.6 GW load increase—to test the system's resilience under different stress conditions. Python was extensively used for processing and presenting results, leveraging PowerFactory's export capabilities, with Excel utilized for consistent system parameter implementation.

## III. GRID-FORMING CONTROL ARCHITECTURES

This section provides an analysis of the controller blocks implemented to represent the GFM controllers. The examination is centered on the three GFM controller types, selected based on the availability of their templates within the PowerFactory software, which facilitates an efficient assessment of their effects on system behavior. The Virtual Synchronous Machine (VSM) and Syncroverter, although often categorized together due to their operational similarities, are treated separately in this discourse to maintain consistency with PowerFactory's naming conventions.

The subsequent subsections highlights the operational principles, mathematical formulations, and control strategies for each controller type, with due acknowledgment of the source material that has informed this analysis [39].

### A. VIRTUAL SYNCHRONOUS MACHINE (VSM)

Virtual Synchronous Machines (VSMs) are devised to provide the system with virtual inertia, mirroring the stabilizing properties of mechanical inertia inherent in traditional synchronous power generation [39]. The VSM's primary function is to simulate the inherent kinetic energy storage of large rotating generators, which is pivotal for system stability during transient disturbances by mitigating abrupt frequency variations [39].

Fig. 4 illustrates the VSM's control system, with the inertia emulation mechanism highlighted. This mechanism is predicated on a reconfigured swing equation, which is adapted to the control inputs comparable to those of conventional synchronous generators.

The classical swing equation is expressed as:

$$\frac{2H}{\omega_0}\frac{d\omega}{dt} = P_m - P_e \tag{5}$$

where $\frac{2H}{\omega_0}$ symbolizes the inertia constant, correlating the generator's angular velocity with the balance of mechanical and electrical power. Disparities in power lead to a modification in angular velocity, which is moderated by the generator's aggregate inertia.

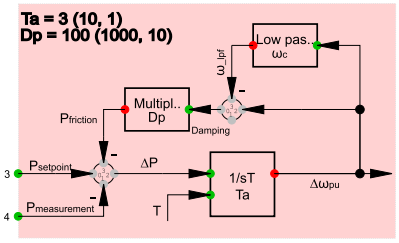


FIGURE 4. **VSM Control Block [39].**

For the VSM, the adapted swing equation is:

$$T_a s\omega = (P_{\text{ref}} - P) - D_p(\omega - \omega_{\text{ref}}) \tag{6}$$

In this equation, $T_a$ denotes the acceleration time constant, and $D_p$ signifies the damping factor. These parameters are critical to the VSM's control approach.

### B. SYNCHROVERTER CONTROL

The synchroverter control scheme is inspired by the governing equations of synchronous machines, particularly the swing equation, but with a focus on torque rather than power, distinguishing it from the VSM approach. It mirrors the frequency droop methodology of traditional synchronous generators, employing a dual-loop control system that encompasses frequency and voltage regulation, denoted in red and blue in Fig. 5, respectively.

The frequency control loop is based on:

$$D_p = -\frac{\Delta T}{\Delta \theta} \tag{7}$$

which leads to the control equation:

$$T_a s\omega = (T_{\text{ref}} - T) - D_p(\omega - \omega_{\text{ref}}) \tag{8}$$

The voltage control loop is governed by:

$$D_q = -\frac{\Delta Q}{\Delta v} \tag{9}$$

and is implemented in the control system as:

$$K_q = D_q(v_{ref} - v) + (Q_{ref} - Q) \tag{10}$$

The synchroverter's control dynamics are characterized by parameters such as the acceleration time constant $T_a$, the damping coefficient $D_p$, the voltage control gain $K_q$, and the reactive power droop coefficient $D_q$.

### C. DROOP CONTROL

The droop control methodology is represented by a frequency-droop controller. The Droop control approach is a well-established approach typically used in microgrids, enabling decentralized control without reliance on communication infrastructures. This strategy is similar to the droop characteristics of traditional synchronous generators but typically known for its slower transient response and power distribution [39].

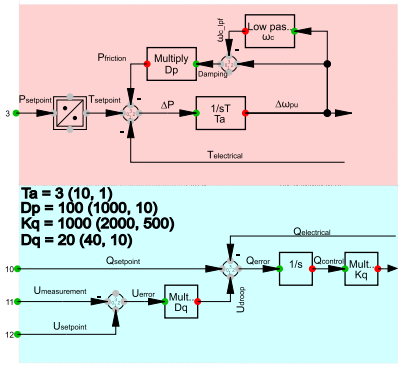


FIGURE 5. **Synchroverter Control Block [39].**

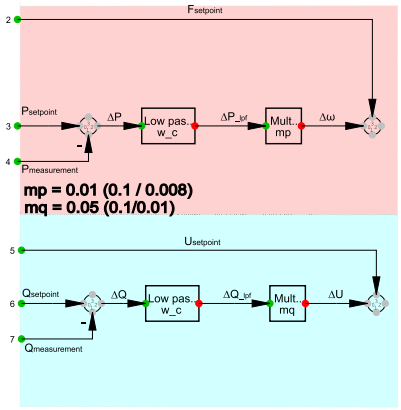


FIGURE 6. **Droop Control Block [39].**

The control block diagram is presented in Fig. 6, with the power-frequency and reactive power-voltage controls highlighted in red and blue, respectively.

The power-frequency control is defined by:

$$\Delta\omega = m_p \Delta P \tag{11}$$

and is translated into the control system as:

$$\omega_{gen} = \omega_{ref} - m_p(P_{out} - P_{in}) \tag{12}$$

Similarly, the reactive power-voltage control is described by:

$$\Delta v = m_q \Delta Q \tag{13}$$

and is represented in the control system as:

$$V = V_{ref} - m_q(Q_{out} - Q_{in}) \tag{14}$$

The droop control scheme fundamentally associates frequency shifts with active power adjustments, and voltage fluctuations with reactive power changes. The principal control parameters include the active power droop coefficient $m_p$ and the reactive power droop coefficient $m_q$. Notably, the droop controller does not contain logic to mimic the inertia similar to the VSM and synchroverter.

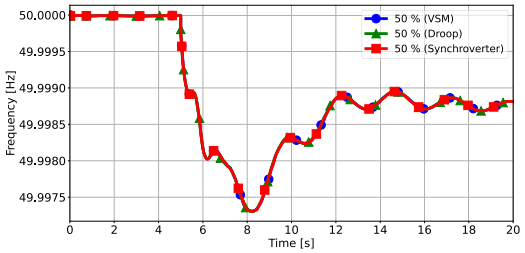


**FIGURE 7.** Frequency response for different GFM controllers with 50% GFM penetration following an outage event occurring at 5 seconds.

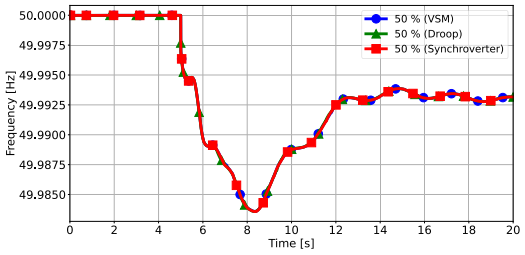


**FIGURE 8.** Frequency response for different GFM controllers with 50% GFM penetration following a load event occurring at 5 seconds.

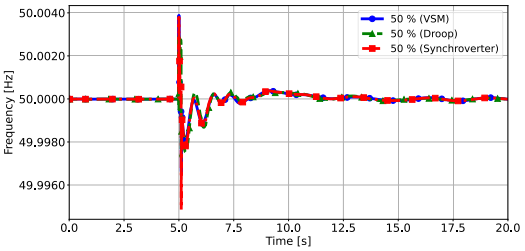


**FIGURE 9.** Frequency response for different GFM controllers with 50% GFM penetration following a short-circuit event occurring at 5 seconds.

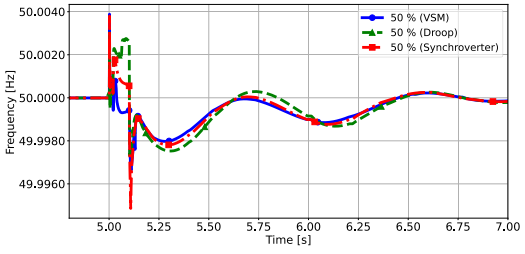


**FIGURE 10.** Frequency response for different GFM controllers with 50% GFM penetration following a short-circuit event occurring at 5 seconds (zoomed view).

## IV. GFM CONTROLLER SELECTION STUDY

The first study compared the VSM, Droop, and Synchroverter controllers across the three events for the three different penetration levels. The results from the 50% penetration levels are given in subsection A.

All three controllers showed nearly identical frequency responses for the load and outage events, with minimal differences in frequency nadir, ROCOF, and maximum deviation

**TABLE 1.** Frequency parameters for the three controller comparisons with GFM penetration.

| Outage Event | | | | |
|---|---|---|---|---|
| Case Index | Frequency Nadir (Hz) | ROCOF (mHz/s) 100 ms | ROCOF (mHz/s) 500 ms | Frequency Deviation (mHz) |
| VSM | 49.9973 | 1.4 | 1.0 | 2.7 |
| Droop | 49.9973 | 1.4 | 1.0 | 2.7 |
| Synchroverter | 49.9973 | 1.2 | 1.0 | 2.7 |
| **Short-Circuit Event** | | | | |
| Case Index | Frequency Nadir (Hz) | ROCOF (mHz/s) 100 ms | ROCOF (mHz/s) 500 ms | Frequency Deviation (mHz) |
| VSM | 49.9961 | 16.1 | 6.3 | 3.9 |
| Droop | 49.9970 | 26.6 | 5.5 | 3.0 |
| Synchroverter | 49.9949 | 33.1 | 9.8 | 5.1 |
| **Load Event** | | | | |
| Case Index | Frequency Nadir (Hz) | ROCOF (mHz/s) 100 ms | ROCOF (mHz/s) 500 ms | Frequency Deviation (mHz) |
| VSM | 49.9836 | 6.6 | 4.9 | 16.4 |
| Droop | 49.9836 | 5.8 | 4.7 | 16.4 |
| Synchroverter | 49.9836 | 6.2 | 4.8 | 16.4 |

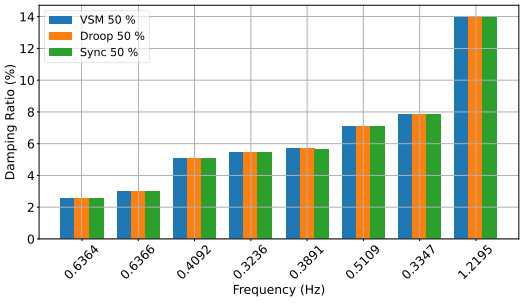


**FIGURE 11.** Damping ratio and frequency for the most critical modes for the three different controllers comparison.

across all penetration levels. This suggests that controller selection has little impact on large-scale system stability for these events. The level of GFM penetration did not significantly affect the frequency response differences among controllers.

However, the short-circuit event showed notable differences. The VSM controller exhibited the lowest frequency deviation during the first swing, followed by the Droop controller, with the Synchroverter displaying the highest. After fault clearance, the Synchroverter again showed the highest deviations. Indicating an overall worse short-circuit capability. Similar patterns were observed at 25% and 85% penetration levels, with the Synchroverter requiring an increase in the maximum allowed short-circuit current to maintain simulation capability at 85% penetration level.

A key difference between the Synchroverter and the VSM controller is the presence of a dedicated voltage control loop. In the VSM controller, this function is managed externally from the outer control structure, whereas in the Synchroverter, it is integrated directly within the control scheme. This distinction influences the short-circuit performance, as voltage fluctuations during fault conditions may

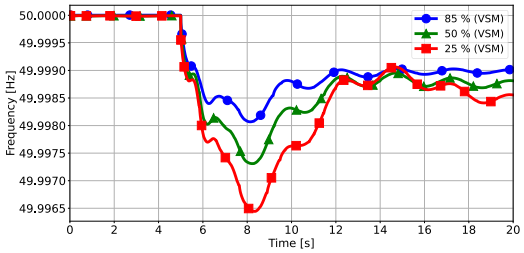


FIGURE 12. **Frequency response for different GFM penetration levels with the VSM controller following an outage event occurring at 5 seconds.**

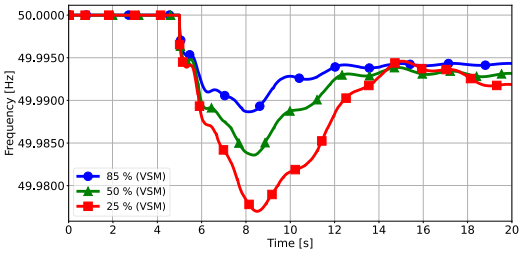


FIGURE 13. **Frequency response for different GFM penetration levels with the VSM controller following a load event occurring at 5 seconds.**

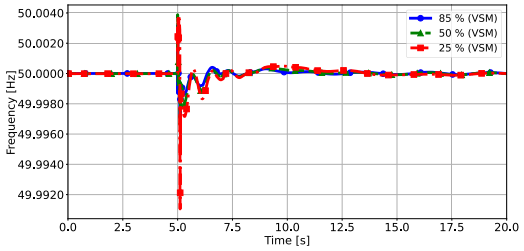


FIGURE 14. **Frequency response for different GFM penetration levels with the VSM controller following a short-circuit event occurring at 5 seconds.**

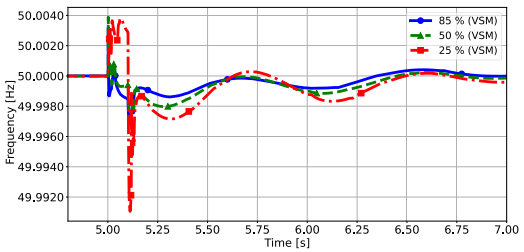


FIGURE 15. **Frequency response for different GFM penetration levels with the VSM controller following a short-circuit event occurring at 5 seconds (zoomed view).**

adversely affect the Synchroverter's response, depending on the dynamic properties of the system under study. In this case, the impact is notably negative, but with optimal controller tuning, this characteristic could potentially be leveraged to improve the dynamic performance. Future investigation is required to examine this hypothesis.

Overall, the frequency analysis revealed minimal differences among controllers for load increases and outages but significant differences in short-circuit scenarios. The VSM and Droop controllers performed better, with the Synchroverter showing the worst performance, particularly at higher penetration levels.

The eigenvalue analysis indicated nearly identical oscillatory performance for all three controllers, with minor deviations in specific oscillatory modes, smaller than 0.1%. This suggests that while theoretical differences exist, their general impact on oscillatory performance is similar.

The various modes are dependent on their frequencies. The modes in the range of 0.63 Hz are intra-area controller modes of the GFL controllers, the modes ranging from 0.32 to 0.51 Hz are inter-area modes dominated by the interconnections and the mode in the range of 1.2 Hz is related to a local mode of controller interactions. These were identified using a participation analysis in PowerFactory.

The similar results between the controllers is notable given the differing control strategies, particularly the absence of synthetic inertia in the Droop controller. Comparing this to the findings in [39] which reported worse performance during load events for the Droop controller, the outcome suggests a distinction worth further investigation. A preliminary explanation is that large-scale systems, even with high PEI penetration retain synchronous inertia that mitigates performance differences across controllers and the lack of synthetic inertia. This could have a larger impact in systems with even lower inertia levels.

While synthetic inertia is often assumed to improve system response, it primarily governs the rate of active power injection based on frequency deviation. Consequently, a Droop-based approach, which directly links active power to frequency, can achieve comparable performance. However, synthetic inertia control may offer advantages for more precise power injection under certain conditions.

Overall, controller choice had a limited impact on large-scale system performance during load and outage events, with short-circuit behavior, particularly in the Synchroverter warranting further study. Although large-scale effects are minimal, local performance differences could play a more significant role in guiding controller selection.

## V. GFM CONVERTER PENETRATION LEVEL ANALYSIS

The second study analyzed the impact of different GFM converter penetration levels on system stability. The study analyzed the three different levels, 25, 50 and 85% for all three controllers.

All three controllers displayed similar performance; thus, only the VSM results are present in subsection A. These figures illustrate frequency responses, damping ratio of different modes and a frequency parameter comparison for the different GFM penetration levels for the different events.

Higher GFM penetration significantly improved the frequency response for the outage event, resulting in lower frequency deviation. While all signals exhibit a similar

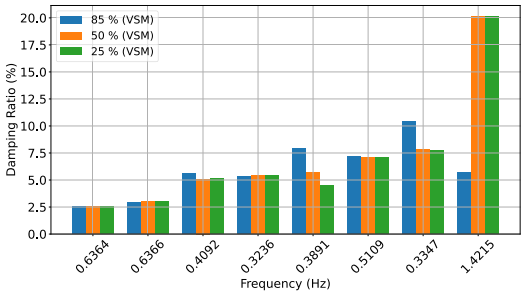


**FIGURE 16.** Damping ratio and related frequency for different penetration levels for the VSM controller.

**TABLE 2.** Frequency parameters for different levels of GFM penetration with the VSM controller.

| Outage Event | | | | |
|---|---|---|---|---|
| VSM Controller | | | | |
| Case Index | Frequency Nadir (Hz) | ROCOF (mHz/s) | | Frequency Deviation (mHz) |
| | | 100 ms | 500 ms | |
| 85% | 49.9981 | 1.0 | 0.7 | 1.9 |
| 50% | 49.9973 | 1.4 | 1.0 | 2.7 |
| 25% | 49.9964 | 1.6 | 1.1 | 3.6 |
| Short-Circuit Event | | | | |
| Case Index | Frequency Nadir (Hz) | ROCOF (mHz/s) | | Frequency Deviation (mHz) |
| | | 100 ms | 500 ms | |
| 85% | 49.9968 | 18.8 | 5.3 | 3.2 |
| 50% | 49.9961 | 16.1 | 6.3 | 3.9 |
| 25% | 49.9911 | 68 | 17.5 | 8.9 |
| Load Event | | | | |
| Case Index | Frequency Nadir (Hz) | ROCOF (mHz/s) | | Frequency Deviation (mHz) |
| | | 100 ms | 500 ms | |
| 85% | 49.9887 | 4.4 | 3.7 | 11.3 |
| 50% | 49.9836 | 6.6 | 4.9 | 16.4 |
| 25% | 49.9770 | 7.2 | 5.8 | 23.0 |

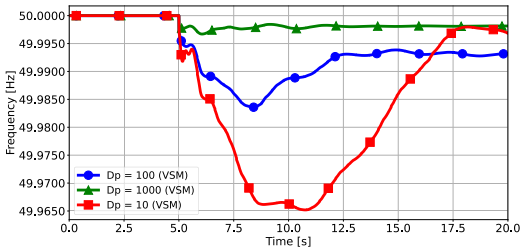


**FIGURE 17.** Frequency response for different $D_p$ values for the VSM controller following a load event occurring at 5 seconds.

oscillatory response, the magnitude of frequency deviations is larger, favoring higher GFM levels. The 85% and 50% penetration levels show a more settled response, while the 25% level exhibits another deviation towards the end of the simulation. ROCOF, frequency nadir, and maximum deviation show minimal differences, with higher penetration levels improving response and settling.

**TABLE 3.** Frequency parameters for different $D_p$ values for the VSM controller.

| $D_p$ (VSM) | | | | |
|---|---|---|---|---|
| Case Index | Frequency Nadir (Hz) | ROCOF (mHz/s) | | Frequency Deviation (mHz) |
| | | 100 ms | 500 ms | |
| $D_p = 100$ | 49.9836 | 6.6 | 4.9 | 16.4 |
| $D_p = 1000$ | 49.9967 | 7.4 | 2.2 | 3.3 |
| $D_p = 10$ | 49.9652 | 17.6 | 7.4 | 34.8 |

A similar pattern was observed for the load response, where higher GFM penetration levels resulted in better frequency stability. The 85% and 50% penetration levels perform better, while the 25% level shows more significant deviations. The load event has a more considerable impact on frequency stability, with higher GFM levels handling disturbances more effectively.

For the short-circuit event, the lowest GFM penetration levels resulted in the highest frequency deviation. The 85% level shows the smoothest response, while the 25% level has a higher oscillatory response after short-circuit clearance.

Overall, higher penetration levels consistently provide better frequency performance across all events for all controllers. Similar findings was found for the Synchroverter and Droop controllers. However, at the highest penetration levels, the Synchroverter required an increased maximum short-circuit current from 1.2 to 1.3 p.u for simulations to converge during the short-circuit event.

The eigenvalue analysis across different penetration levels showed more significant differences than the controller comparison. Higher penetration levels generally improved damping ratios across multiple modes, with only minor reductions in a few modes, which were negligible compared to the overall improvements.

However, a 1.4215 Hz mode showed reduced damping at the highest penetration level. This mode, dominated by a single GFL converter, Disappeared when the converter was removed from the system, indicating it was a local phenomenon. It is likely caused by the fast-acting response of GFM converters in the high-penetration scenario, creating oscillations as the GFL converter struggled to keep up. This behavior occurred with both the Synchroverter and Droop controllers, indicating a consistent pattern.

The reduced damping of this local mode highlights a potential stability risk from high penetration levels under certain topologies. This emphasizes the need for thorough studies to understand these controllers' intrinsic behaviors.

Higher GFM penetration levels generally improved frequency response and oscillatory damping. However, the emergence of a local mode at the highest penetration level highlights potential stability challenges. This finding underscores the need for further research into the intrinsic behavior of GFM—dominated systems, particularly their interactions with GFL converters.

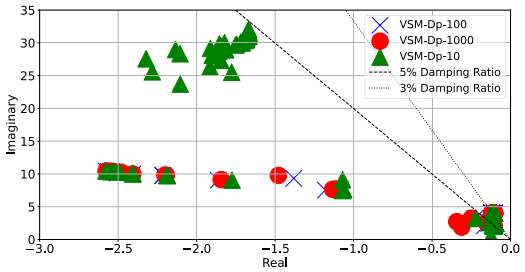


FIGURE 18. Eigenvalues for different $D_p$ values for the VSM controller.

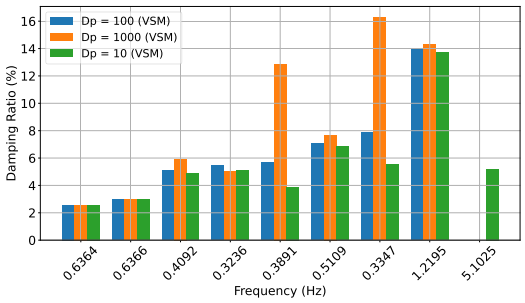


FIGURE 19. Damping ratio and corresponding frequency for different $D_p$ values for the VSM controller.

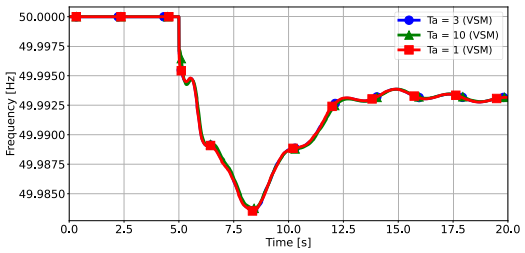


FIGURE 20. Frequency response for different $T_a$ values for the VSM controller following a load event occurring at 5 seconds.

TABLE 4. Frequency parameters for different $T_a$ values for the VSM controller.

| $T_a$ (VSM) | | | | |
|---|---|---|---|---|
| Case Index | Frequency Nadir (Hz) | ROCOF (mHz/s) | | Frequency Deviation (mHz) |
| | | 100 ms | 500 ms | |
| $T_a = 3$ | 49.9836 | 6.6 | 4.9 | 16.4 |
| $T_a = 10$ | 49.9838 | 5.6 | 4.6 | 16.2 |
| $T_a = 1$ | 49.9838 | 5.6 | 4.6 | 16.2 |

## VI. GFM CONTROLLER PARAMETER SENSITIVITY ANALYSIS

The third study analyzed the impact of different controller parameters and their impact on system stability and integrity. Understanding how controller parameters affect system stability in large-scale systems is crucial for future regulatory assessments and tuning of GFM controllers. A load increase was used to evaluate the frequency and oscillatory behavior.

For the VSM controller, the primary parameters analyzed were the acceleration time constant ($T_a$) and the damping coefficient ($D_p$). The simulation results are given in paragraph a. The $D_p$ parameter significantly impacted system stability, with higher $D_p$ values resulting in better frequency response and faster power balancing. The lowest $D_p$ value showed the worst performance, with large frequency deviations and slower settling times. ROCOF, frequency deviation, and frequency nadir for the different values confirmed these findings. The eigenvalue analysis supported this, showing better damping of critical modes with higher $D_p$ values. However, the lowest value of $D_p$ also showed the creation of a local controller mode of 5.1025 Hz, with a damping ratio below 5%. Highlighting the sensitivity and importance of proper controller tuning.

The $T_a$ parameter had minimal impact on system stability, with only slight differences in frequency response and damping. Higher $T_a$ values provided marginally improved damping in high-speed modes, but the overall effect was

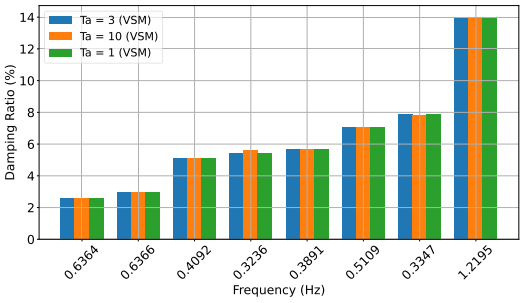


FIGURE 21. Damping ratio and corresponding frequency for different $T_a$ values for the VSM controller. The VSM frequency control loop is highlighted in pink.

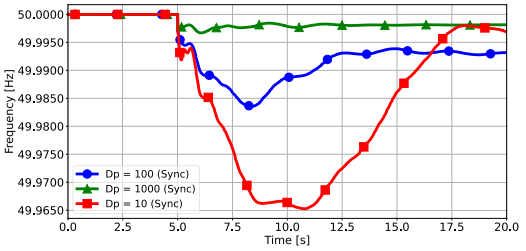


FIGURE 22. Frequency response for different $D_p$ values for the Synchroverter controller following a load event occurring at 5 seconds.

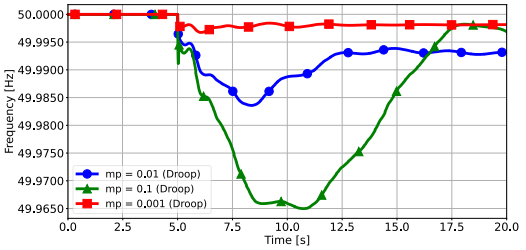


FIGURE 23. Frequency response for different *mp* values for the Droop controller following a load event occurring at 5 seconds.

**TABLE 5. Frequency parameters for different *mp* values for the droop controller.**

| $mp$ (Droop) | | | | |
|---|---|---|---|---|
| Case Index | Frequency Nadir (Hz) | ROCOF (mHz/s) | | Frequency Deviation (mHz) |
| | | 100 ms | 500 ms | |
| $mp = 0.01$ | 49.9836 | 5.8 | 4.7 | 16.4 |
| $mp = 0.1$ | 49.965 | 25.7 | 7.9 | 35.0 |
| $mp = 0.001$ | 49.9967 | 7.3 | 2.1 | 3.3 |

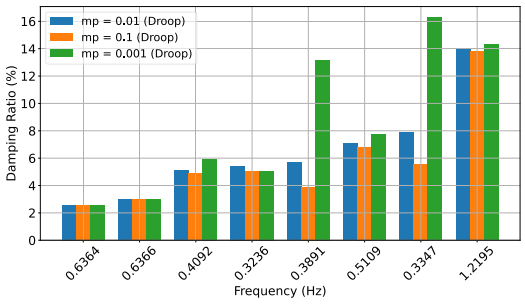


**FIGURE 24. Damping ratio and corresponding frequency for different *mp* values for the Droop controller.**

negligible. This contrasts with prior findings in [39], where $T_a$ significantly affected oscillatory performance in VSM and Synchroverter controllers, with lower values causing increased oscillations and slower damping.

The reduced impact observed here is likely due to the large-scale system model, where multiple synchronous generation sources dominate system inertia, minimizing the influence of synthetic inertia. Notably, this scenario assumed high system inertia; in lower-inertia systems, $T_a$ could have a more pronounced effect.

For the Synchroverter controller, results are given in paragraph b. Here, the $D_p$ parameter had a similar impact as in the VSM controller, with higher values leading to better system stability. Similar to the VSM, a new mode was discovered at the lowest $D_p$ level with low damping. The $T_a$, $K_q$, and $D_q$ parameters showed minimal impact on system stability, indicating possibility for adjustments without affecting oscillatory performance.

The Droop controller's *mp* and *mq* parameters were also analyzed, given in paragraph c. Lower *mp* values resulted in better frequency response, similar to the $D_p$ parameter in the VSM and Synchroverter controllers, except inverted, as the *mp* is initialized as an inverted droop. Interestingly, the *mp* changes did not result in a new mode with low damping unlike the VSM and Synchroverter. This indicates that the Droop controller might be more robust with regards to parameter sensitivities, but further studies is needed to confirm this. The *mq* parameter had no significant impact on system performance, confirming its separation from the active power control loop.

Overall, the main active-power controller parameters ($D_p$ and *mp*) significantly impacted system damping and frequency response. Positive for optimal values and negative for suboptimal values. In contrast, the $T_a$ parameter had a minimal effect, and reactive power control parameters ($K_q$, $D_q$, *mq*) did not affect system stability. This analysis highlights the importance and possibilities of parameter tuning in future systems with high GFM penetration levels.

## VII. CONCLUSION

This paper provides a comprehensive analysis of GFM converters, focusing on controller comparisons, varying levels of GFM penetration, and the influence of converter parameters on large-scale system stability. The paper delves into frequency and oscillatory behavior, using key metrics to draw comparisons.

The controller parameter analysis revealed that the VSM, Droop, and Synchroverter controllers exhibited nearly identical performance in frequency and oscillatory behavior during load and outage events. Minimal differences were observed in Frequency Nadir, ROCOF, maximum frequency deviations, and damping ratios. However, the short-circuit analysis highlighted significant deviations in frequency response across different GFM penetration levels. The Droop controller performed best, followed by the VSM. The Synchroverter showed the worst performance, particularly at 85% penetration, where short-circuit strength became non-viable without increasing the maximum allowed current.

This outcome is notable given the structural similarities between the Synchroverter and VSM controllers, especially in their active power control. Although no conclusive reason for the Synchroverter's worse performance was found, it is hypothesized that the additional reactive power control loop, absent in the VSM, may contribute to its poorer short-circuit response. This extra control layer could create a different dynamic response under fault conditions, affecting short-circuit performance.

These findings suggest that while GFM controller performance remains consistent during load and outage events, short-circuit events can be a key differentiator, highlighting the impact of control structures on stability.

The comparison of GFM penetration levels (25%, 50%, and 85%) indicated that higher penetration levels generally improve frequency response and oscillatory performance for all three controllers. Higher penetration allowed for lower maximum frequency deviations and ROCOF values across all perturbation events, with the most pronounced differences seen during short-circuit events. However, the Synchroverter's limitations at higher short-circuit current levels were again evident. In terms of oscillatory performance, higher penetration levels improved the damping ratios of inter-area modes. However, a local mode in one GFL converter exhibited low damping at the highest penetration level, pointing to potential controller interactions and stability concerns. These findings emphasize the need for further

research to fully understand the dynamics of high GFM penetration levels and their impact on system stability.

The controller parameter analysis demonstrated significant variations based on different controllers and their respective parameters. The main active power parameters ($D_p$ for VSM and Synchroverter and *mp* for Droop) were identified as critical for frequency and oscillatory performance. Adapting these parameters enhanced the damping ratios of inter-area modes, with all modes achieving damping ratios above 5% at the highest parameter values. Conversely, poor parameter tuning resulted in lower damping ratios and the emergence of low-damped modes for the VSM and Synchroverter, underscoring the importance of proper parameter tuning. The acceleration time constant $T_a$ had minimal impact, though slightly better damping in high-speed oscillatory modes was observed. Reactive power control parameters ($K_q$ and $D_q$ for Synchroverter and *mq* for Droop) showed no significant impact on system stability, indicating effective separation of the active and reactive power control loops. However, the controller parameter analysis was only done for the load event, and especially the short-circuit event could have a large influence by the reactive power control parameters.

This paper provides valuable insights into GFM converters, their controller selection, penetration levels, and parameter adjustments. While GFM converters show significant potential in enhancing system stability, certain issues, particularly at high penetration levels and specific controller parameters, suggest their full potential is not yet fully understood. Continued research will be essential for successfully integrating large-scale PEI generation in future power systems.

The results presented for different controllers might be specific to the generic models in PowerFactory and should not be considered representative of all GFM controller types. Models with different control loops, particularly proprietary OEM models, may yield different outcomes. Additionally, as this study is based on a model of the future Dutch power system, the findings may not be directly transferable to other systems, as outcomes can vary depending on system characteristics and future planning decisions, which influence system strength and stability.

The system model used also exhibited some susceptibility to instabilities before the analysis, particularly during short-circuits, due to high PEI generation with low short-circuit capacity. However, it demonstrated good frequency stability, driven by the large amounts of installed generation. Despite these limitations, the results provide a valuable benchmark for large-scale system studies, offering insights into the impact of different GFM parameterizations and implementations.

This study contributes to bridging the gap between research and large-scale system implementation of GFM converters. By analyzing the effects of various parameterizations, it enhances understanding of their behavior in future power systems. The findings provide important insights to guide further research on system stability and inform planning strategies for 2050 and beyond.

Future work should focus on developing and validating intelligent control strategies for GFM converters. Additionally, there is a significant opportunity to explore dynamic control settings, aiming to optimize stability under various operational conditions. This could involve adaptive algorithms that respond in real time to changes in grid dynamics. Another valuable area of research would be to assess the impact of integrating different flexibility resources, such as energy storage systems and demand response, in combination with GFM converters. It is also recommended to recreate a similar analysis for different inertia levels, to better understand the impact of GFM converters under different operational characteristics. Evaluating their combined effect in future energy scenarios will be critical to ensuring a reliable and robust power system that can meet evolving demands and withstand potential disturbances.

## REFERENCES


[1] F. Kaspar, M. Borsche, U. Pfeifroth, J. Trentmann, J. Drücke, and P. Becker, "A climatological assessment of balancing effects and shortfall risks of photovoltaics and wind energy in Germany and Europe," *Adv. Sci. Res.*, vol. 16, pp. 119–128, Jul. 2019, doi: 10.5194/asr-16-119-2019.

[2] P. Tielens and D. Van Hertem, "The relevance of inertia in power systems," *Renew. Sustain. Energy Rev.*, vol. 55, pp. 999–1009, Mar. 2016, doi: 10.1016/j.rser.2015.11.016.

[3] J. Shair, H. Li, J. Hu, and X. Xie, "Power system stability issues, classifications and research prospects in the context of high-penetration of renewables and power electronics," *Renew. Sustain. Energy Rev.*, vol. 145, Jul. 2021, Art. no. 111111, doi: 10.1016/j.rser.2021.111111.

[4] S. Sahoo and P. Timmann, "Energy storage technologies for modern power systems: A detailed analysis of functionalities, potentials, and impacts," *IEEE Access*, vol. 11, pp. 49689–49729, 2023, doi: 10.1109/ACCESS.2023.3274504.

[5] S. Vahidi, M. Ghafouri, M. Au, M. Kassouf, A. Mohammadi, and M. Debbabi, "Security of wide-area monitoring, protection, and control (WAMPAC) systems of the smart grid: A survey on challenges and opportunities," *IEEE Commun. Surveys Tuts.*, vol. 25, no. 2, pp. 1294–1335, 2nd Quart., 2023, doi: 10.1109/COMST.2023.3251899.

[6] J. Rodriguez, F. Blaabjerg, and M. P. Kazmierkowski, "Energy transition technology: The role of power electronics," *Proc. IEEE*, vol. 111, no. 4, pp. 329–334, Apr. 2023, doi: 10.1109/JPROC.2023.3257421.

[7] S. A. Khan, M. Wang, W. Su, G. Liu, and S. Chaturvedi, "Grid-forming converters for stability issues in future power grids," *Energies*, vol. 15, no. 14, p. 4937, Jul. 2022, doi: 10.3390/en15144937.

[8] H. Pishbahar, F. Blaabjerg, and H. Saboori, "Emerging grid-forming power converters for renewable energy and storage resources integration—A review," *Sustain. Energy Technol. Assessments*, vol. 60, Dec. 2023, Art. no. 103538, doi: 10.1016/j.seta.2023.103538.

[9] L. Meegahapola, A. Sguarezi, J. S. Bryant, M. Gu, E. R. Conde, and R. B. A. Cunha, "Power system stability with power-electronic converter interfaced renewable power generation: Present issues and future trends," *Energies*, vol. 13, no. 13, p. 3441, Jul. 2020, doi: 10.3390/en13133441.

[10] R. Hesse, D. Turschner, and H.-P. Beck, "Microgrid stabilization using the virtual synchronous machine (VISMA)," in *Proc. Int. Conf. Renew. Energies Power Quality (ICREPQ)*, Valencia, Spain, Apr. 2009, pp. 15–17.

[11] M. A. Uddin Khan et al., "Comparative evaluation of dynamic performance of a virtual synchronous machine and synchronous machines," in *Proc. 9th Renew. Power Gener. Conf. (RPG)*, vol. 2021, Mar. 2021, pp. 366–371, doi: 10.1049/icp.2021.1362.

[12] H. Alrajhi Alsiraji and R. El-Shatshat, "Comprehensive assessment of virtual synchronous machine based voltage source converter controllers," *IET Gener., Transmiss. Distrib.*, vol. 11, no. 7, pp. 1762–1769, May 2017, doi: 10.1049/iet-gtd.2016.1423.

[13] A. B. Askarov, A. A. Suvorov, M. V. Andreev, and A. S. Gusev, "A review and comparison of current trends in virtual synchronous generator's models," in *Proc. IFAC-PapersOnLine*, 2022, vol. 55, no. 9, pp. 350–355, doi: 10.1016/j.ifacol.2022.07.061.

[14] S. Sproul, S. Cherevatskiy, and H. Klingenberg, "Grid forming energy storage: Provides virtual inertia, interconnects renewables and unlocks revenue," Hitachi ABB Power Grids ElectraNet, Adelaide, Australia, Tech. Rep., Jul. 2020. [Online]. Available: https://www.electranet.com.au/wp-content/uploads/2021/01/Grid-Forming-Energy-Storage-Webinar-ESCRI-SA-July-2020.pdf

[15] S. Sproul et al., "System strength support using grid-forming energy storage to enable high penetrations of inverter-based resources to operate on weak networks," in *Challenges and Advances in Power System Dynamics, C4 System Technical Performance*. Paris, France: CIGRE, 2022.

[16] SINTEF Energy Res. (2024). *Virtual Synchronous Machines*. Accessed: May 28, 2024. [Online]. Available: https://www.sintef.no/en/expertise/sintef-energy-research/virtual-synchronous-machines/

[17] P. V. Thomas. (2022). *Relation Between Torque and Power*. Accessed: Jan. 2, 2024. [Online]. Available: https://www.tutorialspoint.com/relation-between-torque-and-power

[18] (2011). *Power and Torque—Essential Concepts*. Accessed: Jan. 2, 2024. [Online]. Available: http://www.epi-eng.com/piston_engine_technology/power_and_torque.htm

[19] K. R. Vasudevan, V. K. Ramachandaramurthy, T. S. Babu, and A. Pouryekta, "Synchronverter: A comprehensive review of modifications, stability assessment, applications and future perspectives," *IEEE Access*, vol. 8, pp. 131565–131589, 2020, doi: 10.1109/ACCESS.2020.3010001.

[20] L. S. Azuara-Grande, F. Gonzalez-Longatt, G. Tricarico, R. Wagle, S. Arnaltes, and R. Granizo, "Real-time implementation of two grid-forming power converter controls to emulate synchronous generators," in *Proc. IEEE Biennial Congr. Argentina (ARGENCON)*, Sep. 2022, pp. 1–6, doi: 10.1109/ARGENCON55245.2022.9940076.

[21] G. C. Kryonidis, K.-N.-D. Malamaki, J. M. Mauricio, and C. S. Demoulias, "A new perspective on the synchronverter model," *Int. J. Electr. Power Energy Syst.*, vol. 140, Sep. 2022, Art. no. 108072, doi: 10.1016/j.ijepes.2022.108072.

[22] M. Mohamed, F. Dubuisson, B. S. Beram, M. Rezkallah, A. Hamadi, and A. Chandra, "Combination of the synchronverter with droop control for hybrid OFF-grid system," in *Proc. IEEE Int. Conf. Power Electron., Drives Energy Syst. (PEDES)*, Dec. 2022, pp. 1–4, doi: 10.1109/PEDES56012.2022.10080562.

[23] K. R. Vasudevan, V. K. Ramachandaramurthy, G. Venugopal, J. M. Guerrero, and G. D. A. Tinajero, "Synergizing pico hydel and battery energy storage with adaptive synchronverter control for frequency regulation of autonomous microgrids," *Appl. Energy*, vol. 325, Nov. 2022, Art. no. 119827, doi: 10.1016/j.apenergy.2022.119827.

[24] P. Piagi and R. H. Lasseter, "Autonomous control of microgrids," in *Proc. IEEE Power Eng. Soc. Gen. Meeting*, Jul. 2006, p. 8, doi: 10.1109/PES.2006.1708993.

[25] J. Grainger and W. Stevenson, *Power System Analysis*. New York, NY, USA: McGraw-Hill, 1994.

[26] K. Rahman et al., "Reviewing control paradigms and emerging trends of grid-forming inverters—A comparative study," *Energies*, vol. 17, no. 10, May 2024, Art. no. 2400, doi: 10.3390/en17102400.

[27] F. Ibanez, A. Mahmoud, V. Yaroslav, V. Peric, and P. Vorobev, "Improving the power sharing transients in droop-controlled inverters with the introduction of an angle difference limiter," *Int. J. Electr. Power Energy Syst.*, vol. 153, Nov. 2023, Art. no. 109371, doi: 10.1016/j.ijepes.2023.109371.

[28] S. Fazal, M. E. Haque, M. T. Arif, and A. Gargoom, "Droop control techniques for grid forming inverter," in *Proc. IEEE PES 14th Asia Pacific Power Energy Eng. Conf. (APPEEC)*, Nov. 2022, pp. 1–6, doi: 10.1109/APPEEC53445.2022.10072251.

[29] W. Issa, S. Sharkh, and M. Abusara, "A review of recent control techniques of drooped inverter-based AC microgrids," *Energy Sci. Eng.*, vol. 12, no. 4, pp. 1792–1814, Jan. 2024, doi: 10.1002/ese3.1670.

[30] D. B. Rathnayake et al., "Grid forming inverter modeling, control, and applications," *IEEE Access*, vol. 9, pp. 114781–114807, 2021, doi: 10.1109/ACCESS.2021.3104617.

[31] J. Bialek et al., "System needs and services for systems with high IBR penetration," Global Power System Transformation Consortium, Nat. Renew. Energy Lab. (NREL), U.S. Dept. Energy, Tech. Workstream Rep., 2021. [Online]. Available: https://globalpst.org/wp-content/uploads/GPST-IBR-Research-Team-System-Services-and-Needs-for-High-IBR-Networks.pdf

[32] Tennet. (Oct. 2023). *Integrale Infrastructuurverkenning 2030–2050*. [Online]. Available: https://www.tennet.eu/nl/over-tennet/publicaties/integrale-infrastructuurverkenning-2030-2050

[33] TenneT. (2024). *Target Grid*. Accessed: Jan. 25, 2024. [Online]. Available: https://www.tennet.eu/target-grid

[34] TenneT. (2024). *Ontwerpinvesteringsplan Net Op Land 2024–2033*. [Online]. Available: https://tennet-drupal.s3.eu-central-1.amazonaws.com/default/2024-01/IP2024_Netopland_01-1-2024_0.pdf

[35] TenneT. (2024). *Ontwerpinvesteringsplan Net Op Zee 2024-2033*. [Online]. Available: https://tennet-drupal.s3.eu-central-1.amazonaws.com/default/2024-01/IP2024_Netopzee_01-1-2024.pdf

[36] *Inertia and Rate of Change of Frequency (RoCoF) Version 17 SPD—Inertia TF*, ENTSO-E, Brussels, Belgium, Dec. 16, 2020.

[37] *TYNDP 2022 System Needs Study: System Dynamic and Operational Challenges*, ENTSO-E, Brussels, Belgium, May 2023.

[38] *PowerFactory 2023 Technical Reference: DIgSILENT Grid-Forming Converter Templates: Droop Controlled Converter, Synchronverter, Virtual Synchronous Machine*, DIgSILENT GmbH, Gomaringen, Germany, 2023.

[39] S. Skogen, J. R. Torres, and P. Palensky, "Fundamental assessment of oscillatory performance of grid-forming integrated systems," in *Proc. Int. Workshop Artif. Intell. Mach. Learn. Energy Transformation (AIE)*, Vaasa, Finland, May 2024, pp. 1–6, doi: 10.1109/AIE61866.2024.10561388.

**SANDER LID SKOGEN** was born in 1998. He received the B.Eng. degree in electrical engineering, specializing in electric power and sustainable energy from Norwegian University of Science and Technology (NTNU) in 2022, and the joint M.Sc. degree (cum laude) in electrical engineering from Delft University of Technology and Wind Energy, and the EWEM Program, NTNU, in 2024. He is currently an Electrical Engineer with Equinor, working within the Technology, Digital and Innovation (TDI) Department. He began his career as an Electrician, completing his training in 2019. His research interests focus on power system operation and dynamics.

**JOSÉ LUIS RUEDA TORRES** (Senior Member, IEEE) was born in 1980. He received the Diploma degree (cum laude) in electrical engineering from the Escuela Politécnica Nacional, Quito, Ecuador, in August 2004, and the Ph.D. degree [Sobresaliente' (Outstanding)] in electrical engineering from the National University of San Juan, in November 2009. He is currently an Associate Professor leading the Research Team on Dynamic Stability of Sustainable Electrical Power Systems, Intelligent Electrical Power Grids Section, Electrical Sustainable Energy Department, Delft University of Technology, Delft, The Netherlands. From September 2003 to February 2005, he was with Ecuador, in the fields of industrial control systems and electrical distribution networks operation and planning. From August 2010 to February 2014, he was a Post-Doctoral Research Associate with the Institute of Electrical Power Systems, University Duisburg-Essen, Duisburg, Germany. His research interests include physics-driven analysis of stability phenomena dynamic equivalencing of HVdc–HVac systems, probabilistic multi-systemic reliability and stability management, and adaptive-optimal resilient multi-objective controller design. He is a member of the Technical Committee on Power and Energy Systems of the International Federation of Automatic Control (IFAC) and the Vice-Chair of the IEEE PES Intelligent Systems Subcommittee and the IFAC Technical Committee TC 6.3. Power and Energy Systems on social media.